EXAFS Debye–Waller Factor and Thermal Vibrations of Crystals

G. Dalba and P. Fornasini

Dipartimento di Fisica dell'Università degli Studi di Trento and Istituto Nazionale di Fisica della Materia, I-38050 Povo (Trento), Italy. E-mail: fornasin@alpha.science.unitn.it

The EXAFS Debye–Waller factor depends on the correlation of atomic motion and can yield original information on the vibrational dynamics of crystalline solids. In this paper an introductory treatment of thermal disorder in EXAFS, based on the cumulant approach, is given. The general relation between mean-square relative displacement (MSRD) measured by EXAFS and atomic thermal vibrations in harmonic approximation is explored. Strengths and limitations of the phenomenological Einstein- and Debye-correlated models are discussed. Some of the most significant results so far obtained are reviewed. A relatively simple method for estimating anharmonic corrections to the MSRD is proposed.

1. Introduction

The amplitude and phase of EXAFS oscillations are influenced by local disorder of thermal and static origin. EXAFS is generally more sensitive to disorder than X-ray diffraction (XRD) because of the higher values of momentum transfer $2k$, k being the photoelectron wavevector. This sensitivity to disorder, added to the unavailability of low-k data, represents a drawback in structural investigations beyond the short-range order. It can instead be positively exploited, thanks also to the relative easiness of temperature-dependent EXAFS measurements, to gain original information on local vibrational dynamics of both crystalline and non-crystalline solids and on local structural distortions.

The effect of disorder on the amplitude of the EXAFS signal is generally accounted for by an EXAFS Debye–Waller factor $\exp(-2k^2\sigma^2)$, where σ^2 is the mean-square relative displacement (MSRD) of absorber and backscatterer atoms (Lee, Citrin, Eisenberger & Kincaid, 1981). The peculiar sensitivity of the MSRD to the correlation of vibrational motion in crystals was recognized early on (Shmidt, 1961, 1963; Beni & Platzman, 1976; Sevillano, Meuth & Rehr, 1979), suggesting the use of EXAFS for checking the phase relationships between eigenvectors of the dynamical matrix obtained from *ab-initio* or model calculations. On more general grounds the temperature dependence of the MSRD provides a measure of the effective bond-stretching force constant between absorber and backscatterer atoms, and can be utilized for studying the strengths of chemical bonds. As a further enhancement of the potentialities of EXAFS it was shown that the analysis of spectra by the cumulant expansion method (Bunker, 1983) allows one, in principle, to single out and quantify the anharmonic contributions to the MSRD (Dalba, Fornasini, Gotter &

Rocca, 1995; Dalba, Fornasini, Grazioli & Rocca, 1995), leading to a more accurate comparison with theoretical calculations based on the harmonic approximation.

A general procedure to take into account the effects of thermal and static disorder in multiple-scattering contributions was developed by Benfatto, Natoli & Filipponi (1989). A method to calculate the EXAFS Debye–Waller factor in the case of weak anharmonicity, based on a first principles quantum statistical approach, was presented by Fujikawa & Miyanaga (1993).

In spite of these considerations and with the exception of a few pioneering studies (Böhmer & Rabe, 1979; Greegor & Lytle, 1979; Sandstrom, Marques, Biebesheimer, Lytle & Greegor, 1985; Knapp, Pan & Tranquada, 1985; Balerna & Mobilio, 1986), only occasional use has been made of EXAFS to probe the vibrational properties of solids. An extended compilation of experimental results, including thermal expansion studies, has recently been made by Tröger *et al.* (1994). The scarcity of experimental data has prevented a reliable assessment of the ultimate accuracy attainable in the comparison between the EXAFS Debye–Waller factor and theoretical predictions.

This paper is intended to give an up-to-date introductory account of the effects of thermal disorder on EXAFS, maintaining as much as possible a phenomenological approach. Only crystalline unoriented systems will be considered. A general introduction to the treatment of thermal disorder in EXAFS based on the cumulant expansion method is given in §2, and §3 is dedicated to some peculiar details on measurements and data analysis. The connection between the MSRD and atomic thermal displacements is made in §4: here the general expression of the MSRD in terms of eigenvectors and eigenfrequencies of the dynamical matrix within the harmonic approximation is given; besides, strengths and limitations of the frequently used Einstein-

and Debye-correlated models are explored. In §5 the anharmonic contributions to the MSRD are discussed briefly, and §6 is dedicated to concluding remarks.

2. Disorder in EXAFS

Thermal disorder spreads atomic positions in crystals into tridimensional distributions, which in harmonic approximation are described by Gaussian thermal ellipsoids (Willis & Pryor, 1975). The sampling time of an EXAFS photoelectron ($\sim 10^{-16}$ s) is much shorter than the atomic vibrational periods ($\sim 10^{-13}$ s). An EXAFS experiment samples a unidimensional canonical distribution of instantaneous interatomic distances, $\rho(r)$, for each coordination shell of the absorber atom (Fig. 1). The distribution $\rho(r)$ also contains contributions from structural disorder, site disorder and compositional disorder (Bunker, 1983). In this paper we will consider only thermal disorder.

Within the single-scattering and plane-wave approximations the normalized EXAFS function for one coordination shell of an unoriented sample (such as a crystalline powder) is generally expressed (Crozier, Rehr & Ingalls, 1988) as

$$\chi(k) = (S_0^2 N/k) \, \text{Im}\Big[f(k,\pi) \exp(2i\delta)$$
$$\times \int_0^\infty \rho(r) \exp(-2r/\lambda) \exp(2ikr)/r^2 \, dr\Big], \quad (1)$$

where N is the coordination number, $f(k,\pi)$ is the complex backscattering amplitude and δ is the central atom phase shift. S_0^2 and λ take into account intrinsic and extrinsic anelastic effects, respectively. All the r-dependent factors within (1) are globally referred to as the *effective distribution* of distances

$$P(r,\lambda) = \rho(r) \exp(-2r/\lambda)/r^2. \quad (2)$$

The applicability of (1) in the high-temperature limit and pairwise central force approximation has been confirmed
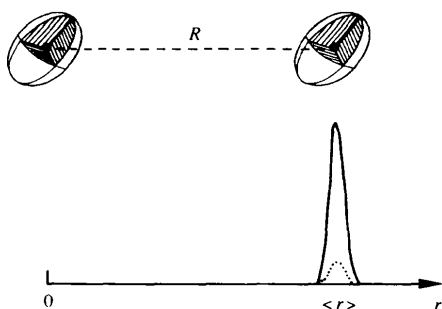

Figure 1
Schematic comparison between the harmonic descriptions of thermal disorder in diffraction (XRD) and EXAFS. The interatomic spacing R is the distance between the centres of thermal ellipsoids (upper part of the figure). An EXAFS experiment samples the unidimensional distribution $\rho(r)$ of instantaneous distances r (lower part, continuous line), whose average value $\langle r \rangle$ is generally larger than R owing to the effect of thermal vibrations normal to the bond direction (Dalba, Fornasini, Gotter & Rocca, 1995). The dashed line represents the effective distribution $P(r,\lambda) = \rho(r) \exp(-2r/\lambda)/r^2$.

by Fujikawa & Miyanaga (1993). The single-scattering approximation can be safely utilized when only the first-shell signal is analyzed. For outer shells, multiple-scattering contributions can be non-negligible. Also, curved-wave effects can be non-negligible in calculations of thermal disorder, particularly when dealing with asymmetric distributions of distances (Brouder, 1988; Rennert, 1992; Fujikawa, Yimagawa & Miyanaga, 1995). However, curved-wave corrections can be to a good extent compensated, for systems with not too high degrees of disorder and asymmetry, if the analysis of data is performed utilizing backscattering amplitudes and phase shifts extracted from an experimental reference, which for vibrational dynamics studies is the same sample measured at very low temperature (see §3.2).

The basic problem of EXAFS analysis is the inversion of (1) in order to recover, from an experimental EXAFS signal $\chi(k)$, the distribution $\rho(r)$, or at least its leading statistical parameters such as mean value and variance. This problem cannot be exactly solved, the main limitation being the lack of the low-k part of the spectrum. Among the different approximate solutions which have been proposed for this problem, the one based on the cumulant expansion is particularly appealing for the treatment of purely thermal disorder.

Basically, the structural part of the EXAFS formula, (1), can be expanded as a MacLaurin series of the wavevector k,

$$\ln \int_0^\infty P(r,\lambda) \exp(2ikr) \, dr = \sum_{n=0}^\infty [(2ik)^n/n!] C_n, \quad (3)$$

where the coefficients C_n are the *cumulants* of the effective distribution $P(r,\lambda)$.

The cumulants C_i are connected to the moments by simple linear relations (Gnedenko, 1976). One advantage of cumulants is their immediate relation with EXAFS formula (1), odd and even cumulants determining phase and amplitude, respectively.

$$\Phi(k) = 2kC_1 - 4k^3 C_3/3 + 4k^5 C_5/15 + \ldots + \varphi, \quad (4)$$

$$A(k) = (S_0^2 N/k)|f(k,\pi)|$$
$$\times \exp(C_0 - 2k^2 C_2 + 2k^4 C_4/3 - 4k^6 C_6/45 + \ldots). \quad (5)$$

A second advantage of cumulants is their simple physical interpretation. C_0 depends on the normalization of the distribution and contains information on λ. C_1 is the mean value, C_2 the variance of the distribution. Higher order cumulants characterize the shape of the distribution: they are zero for Gaussian distributions. The third cumulant, C_3 (and possibly higher-order odd cumulants), depends on the asymmetry of the distribution and is connected to thermal expansion. The fourth cumulant, C_4 (and possibly higher-order even cumulants), describes symmetric deviation from Gaussian shape (Fig. 2).

The convergence of the cumulant series in (3) critically depends on the shape of the distribution (Crozier *et al.*,

1988; Dalba, Fornasini & Rocca, 1993). For small degrees of disorder only the first cumulants (C_0, C_1 and C_2) are significant, the effective distribution of distances can be considered Gaussian and (1) reduces to the *standard formula* for EXAFS in harmonic approximation (Lee *et al.*, 1981):

$$\chi(k) = (S_0^2 N/k)\,|f(k,\pi)|\,[\,\exp\,(-2C_1/\lambda)/C_1^2\,]$$
$$\times\,\exp\,(-2k^2 C_2)\sin\,(2kC_1 + \varphi). \qquad (6)$$

Equation (6) can be safely used for low-temperature spectra (measured at liquid-nitrogen or better liquid-helium temperature), where anharmonicity contributions are negligible. When the Debye temperature is approached, anharmonicity effects cannot be neglected: the Gaussian approximation for the effective distribution is no longer valid and high-order cumulants become important. When the temperature increases further, a larger number of cumulants become significant and eventually the convergence interval of the cumulant series becomes shorter than the EXAFS range. In §3.1 some criteria will be presented to check the convergence properties of the cumulant series, while §5 is dedicated to the treatment of anharmonicity.

Equations (4) and (5) express EXAFS as a function of the cumulants C_i of the *effective* distribution $P(r,\lambda)$, while one is interested in the corresponding cumulants of the *real* distribution $\rho(r)$: $\langle r \rangle$, σ^2, $\sigma^{(3)}$, $\sigma^{(4)}$, ... For small disorder the second- and higher-order cumulants of the effective and real distributions are generally considered equal, within the experimental uncertainties (Bunker, 1983); that is why in the standard formula (6) the *EXAFS Debye–Waller factor*

is directly expressed as $\exp\,(-2k^2\sigma^2)$. For large disorder, however, the difference between the cumulants of the two distributions could be not negligible (Dalba, Fornasini, Gotter & Rocca, 1995).

The difference between the first cumulants of the effective and real distributions, C_1 and $\langle r \rangle$, respectively, is not negligible also for small disorder (Bunker, 1983):

$$C_1 = \langle r \rangle - (2\sigma^2/\langle r \rangle)(1 + \langle r \rangle/\lambda). \qquad (7)$$

For example, it amounts to about 0.002 Å for the first shell of germanium at 300 K, and grows to about 0.01 Å for the first shell of AgI at the same temperature. A consistent difference can exist between the mean value $\langle r \rangle$ of the real distribution and the actual interatomic distance R, owing to the effect of thermal vibrations normal to the bond direction (Eisenberger & Brown, 1979; Ishii, 1992; Dalba, Fornasini, Gotter & Rocca, 1995; Dalba *et al.*, 1996). This difference can be larger than the difference between C_1 and $\langle r \rangle$ and is of opposite sign.

The cumulant expansion of EXAFS has been utilized in several cases for reconstructing the low-k missing part of the experimental spectra and recovering the full distribution of distances by inversion of (1) (Stern, Ma, Hanske-Petitpierre & Bouldin, 1992; Dalba *et al.*, 1993). In cases of poor convergence of the cumulant series the low-k reconstructed EXAFS function can be *spliced* to the high-k experimental spectrum (Crozier *et al.*, 1988; Ono, Yokoyama, Sato, Kaneyuki & Ohta, 1992).

3. Experimental

3.1. Measurements

To gain information on vibrational dynamics of crystalline solids from EXAFS spectra it is necessary to perform temperature-dependent measurements with very high signal-to-noise ratios. The explored range of temperatures depends on the compound examined (in particular its Debye temperature) and the phenomena which one wants to study (correlation of vibrational motion, anharmonicity, phase transitions *etc.*)

A low-temperature spectrum is always necessary, to be used as a harmonic reference if a phenomenological analysis based on the ratio method is planned, or for calibration purposes in case of analysis performed using calculated amplitudes, phase shifts and anelastic terms. Liquid nitrogen can be appropriate for relatively high Debye temperatures (typically higher than 300 K). For lower Debye temperatures a liquid-helium reference should be preferred. The temperature should be measured directly on the sample with an accuracy no worse than ±2 K.

3.2. Data analysis

Various methods for the analysis of EXAFS spectra have been proposed and are currently utilized. In this paper we will consider the phenomenological method based on complex Fourier filtering of the contributions of different
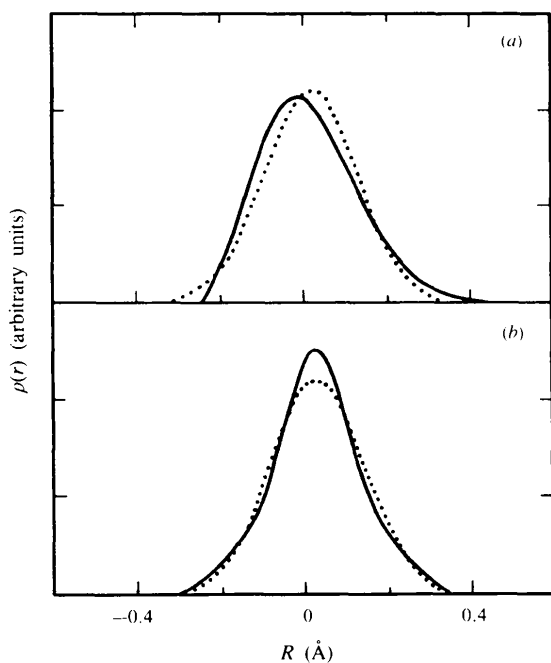

Figure 2
Dotted lines: Gaussian distribution with variance $C_2 = 0.013\ \text{Å}^2$. Continuous lines: distributions obtained by adding to the Gaussian a third cumulant $C_3 = 10^{-3}\ \text{Å}^3$ (*a*) or a fourth cumulant $C_4 = 10^{-4}\ \text{Å}^4$ (*b*).

coordination shells and separate analysis of phase and amplitude by comparison with a low-temperature reference (*phase difference and amplitude ratio method*). The implementation of this method is well documented in the literature (Lee *et al.*, 1981; Bunker, 1983). Here we will emphasize only some relevant points.

Fourier filtering separates the contributions of sufficiently distant coordination shells; this procedure is particularly useful for the first shell, whose signal can be safely treated within the single-scattering approximation. The alternative analysis of the whole unfiltered spectrum would require a multiple-scattering approach, which for the low-temperature EXAFS of a crystal should include a large number of coordination shells and scattering paths. Fourier filtering introduces signal distortions due to finite windows; this effect can be reduced by using the same windows for all analyzed spectra. The residual errors on final parameters can be quantified and possibly reduced by suitable tests on model EXAFS spectra.

For a well separated coordination shell, as a consequence of (4) and (5), the difference of EXAFS phases is

$$\Phi_s(k) - \Phi_r(k) = 2k\Delta C_1 - 4k^3\Delta C_3/3 + 4k^5\Delta C_5/15 - \dots \tag{8}$$

and the logarithm of the amplitudes ratio is

$$\ln[A_s(k)/A_r(k)] = \ln[N_s/N_r + \Delta C_0 - 2k^2\Delta C_2 + 2k^4\Delta C_4/3 - 4k^6\Delta C_6/45 + \dots , \tag{9}$$

where $\Delta C_i = \Delta C_i^s - \Delta C_i^r$, s labelling the spectrum at temperature T, r the low-temperature reference spectrum.

For not too large distributions one can approximate $\exp(C_0) = \exp(-2C_1/\lambda)/C_1^2$, so that

$$\Delta C_0 = -2(C_1^s - C_1^r)/\lambda - 2(\ln C_1^s - \ln C_1^r). \tag{10}$$

This term, often negligible, can be estimated from a rough knowledge of interatomic distance and mean free path.

The main advantage of the method of analysis based on (4) and (5) relies on the elimination of backscattering amplitudes and phase shifts and anelastic terms, and of the errors connected with their calculations. The main drawback is its uselessness when dealing with composite coordination shells. Moreover, one should be very cautious in using this method when non-negligible multiple scattering or curved-wave effects are expected.

The separate analysis of phases and amplitudes, (8) and (9), eliminates the correlation between phase and amplitude parameters. Besides, it allows a direct check of the influence of anharmonicity and, as a consequence, of the applicability of the standard formula, (6): for a Gaussian distribution of distances the plots of phase difference *versus* k and logarithm of amplitude ratio *versus* k^2 must be linear; the deviations from linearity are fingerprints of anharmonicity and suggest that the standard formula should not be used. A working example of the difference between a linear and a non-linear behaviour is shown in Fig. 3.

Polynomial fits to phase differences and logarithms of amplitude ratios give a finite number of polynomial co-

efficients $\Delta \tilde{C}_i$, owing to the criterion that the maximum number of independent parameters obtainable from an EXAFS spectrum is $n_{ind} = 2\Delta k \Delta r/\pi$, where Δk and Δr are the k- and r-space windows, respectively (Lee *et al.*, 1981). The significance of high-degree terms has in any case to be checked in view of the smooth behaviour of the experimental phase differences and amplitude ratios. The amplitude analysis is generally made up to the fourth-degree and exceptionally the sixth-degree term.

Whether the polynomial coefficients obtained from EXAFS analysis are actually a good approximation of the cumulants of the effective distribution depends on the convergence properties of the cumulant series. A test of the correspondence of polynomial coefficients with cumulants can be made by checking the regularity of their temperature dependence (Dalba *et al.*, 1993). To first order, an Einstein-like behaviour is expected for the second cumulant C_2, and a proportionality to T^2 and T^3 for C_3 and C_4, respectively (Tranquada & Ingalls, 1983). An example is given in Fig. 4.

The analysis based on the ratio method gives only *relative* values ΔC_i of the cumulants. If the temperature of the reference spectrum is sufficiently low, the corresponding distribution can be considered Gaussian, so that $C_i^r = 0$ for $i > 2$ and absolute values of third- and higher-order cumulants are directly obtained for high-temperature spectra. As far as the second cumulant is concerned, one generally obtains the absolute values C_2 by fitting an Einstein- or a Debye-correlated model to the slope of the experimental data ΔC_2 and vertically shifting the data to match the theoretical model (Fig. 4). This procedure will be discussed in §§4.5 and 5. The alternative data analysis based on the use of calculated backscattering amplitudes
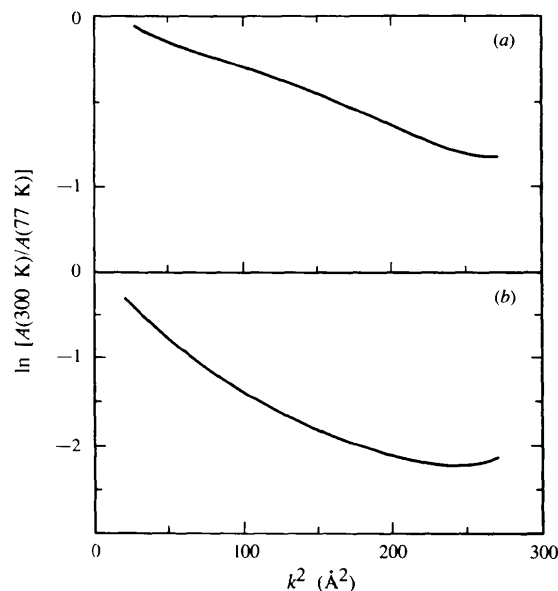

Figure 3

Logarithm of the ratio between EXAFS amplitudes at 300 and 77 K plotted against k^2 for the first shell of c-Ge (*a*) and AgI (*b*). In case (*a*) equation (8) can be safely truncated at the linear term (second cumulant); in case (*b*) higher-order cumulants must be considered.

and phase shifts and anelastic terms directly gives absolute values of cumulants; the accuracy of these values depends, however, on the accuracy of theoretical calculations. A comparative use of both methods of analysis can help in obtaining at the same time accurate and absolute values of the second cumulant (Dalba, Fornasini, Kuzmin, Purans & Rocca, 1995).

4. Mean-square relative displacement

The second cumulant C_2 is the variance of the effective distribution $P(r,\lambda)$. In the case of small disorder it is a good estimate of the variance σ^2 of the distribution $\rho(r)$, e.g. of the mean-square relative displacement of absorber and backscatterer atoms. In this section we will examine the connection between MSRD and vibrational properties of crystalline solids in harmonic approximation.

4.1. MSRD and atomic displacements

Let $\mathbf{R}$ be the vector connecting the centres of the thermal ellipsoids of the absorber atom and one backscatterer atom. The instantaneous interatomic distance, $\mathbf{r}$, is

$$\mathbf{r} = \mathbf{R} + \mathbf{u}_j - \mathbf{u}_0, \tag{11}$$

where $\mathbf{u}_0$ and $\mathbf{u}_j$ are the instantaneous atomic displacements of the absorber and backscatterer atoms, respectively (Fig. 5). The modulus of $\mathbf{r}$ can be expanded in power series

of the atomic displacements (Busing & Levy, 1964),

$$r = R + \Delta u_{\parallel} + (\Delta u_{\perp}^2)/2R + \ldots, \tag{12}$$

where $\Delta u_{\parallel} = \hat{\mathbf{R}} \cdot (\mathbf{u}_j - \mathbf{u}_0)$ is the component of the relative atomic displacement *parallel* to the bond direction, $\Delta u_{\perp}$ the corresponding *normal* component; $\hat{\mathbf{R}}$ is the unit vector.

The mean-square relative displacement of the pair of absorber and backscatterer atoms is the canonical average

$$\sigma_j^2 = \langle (r - R)^2 \rangle \simeq \langle (\Delta u_{\parallel})^2 \rangle = \langle [\hat{\mathbf{R}} \cdot (\mathbf{u}_j - \mathbf{u}_0)]^2 \rangle$$
$$= \langle (\hat{\mathbf{R}} \cdot \mathbf{u}_j)^2 \rangle + \langle (\hat{\mathbf{R}} \cdot \mathbf{u}_0)^2 \rangle - 2\langle (\hat{\mathbf{R}} \cdot \mathbf{u}_j)(\hat{\mathbf{R}} \cdot \mathbf{u}_0) \rangle. \tag{13}$$

To first order the MSRD only depends on the relative atomic displacements parallel to the interatomic vector distance. The MSRD contains the contribution from the mean-square displacements (MSD) of both absorber and backscatterer atoms, $\langle (\hat{\mathbf{R}} \cdot \mathbf{u}_0)^2 \rangle$ and $\langle (\hat{\mathbf{R}} \cdot \mathbf{u}_j)^2 \rangle$, respectively, and the displacement correlation function (DCF) $\langle (\hat{\mathbf{R}} \cdot \mathbf{u}_j)(\hat{\mathbf{R}} \cdot \mathbf{u}_0) \rangle$ (Beni & Platzman, 1976).

4.2. Harmonic approximation

In the harmonic approximation the expansion of the crystal potential, Φ, in series of the atomic displacements is truncated at the second-order term. The vibrational motion of N atoms can be decomposed in $3N$ normal modes, each mode being identified by a wavevector $\mathbf{q}$ and a branch index λ. The instantaneous displacement of the jth atom within
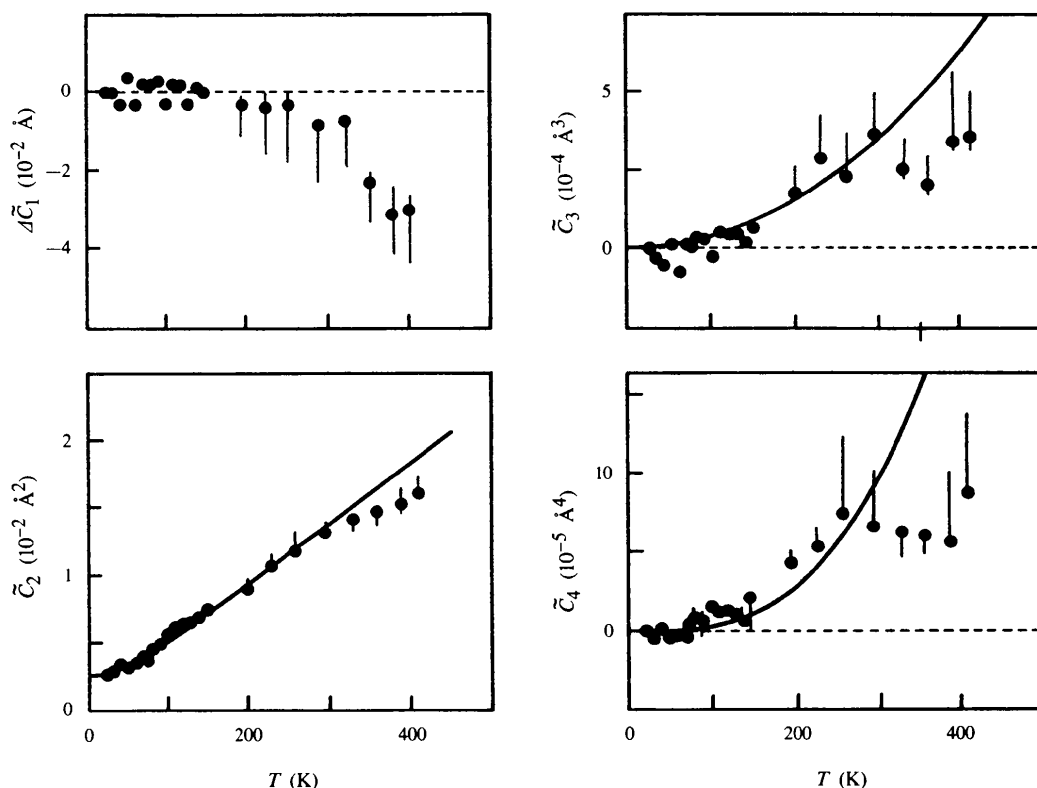

Figure 4

Polynomial coefficients obtained from the analysis of phases and amplitudes of EXAFS at the K edge of Ag in AgI (Dalba *et al.*, 1993). A k range extending to 16 Å^{-1} was considered. A growing discrepancy between polynomial coefficients and the expected behaviour of cumulants (continuous lines) is evident above 300 K, suggesting that the number of coefficients considered is inadequate with respect to the k range. Absolute values of $\bar{C}_2$ were obtained by fitting an Einstein model to the slope of the experimental points.

the nth unit cell can be expressed as (Brüesch, 1982)

$$\mathbf{u}_{nj}(t) = (Nm_j)^{-1/2} \sum_{\mathbf{q},\lambda} Q(\mathbf{q},\lambda,t)\, \mathbf{w}_j(\mathbf{q},\lambda)\, \exp\,(i\mathbf{q}\cdot\mathbf{r}_{nj}), \quad (14)$$

where N is the number of unit cells and m_j and $\mathbf{r}_{nj}$ are the mass and vector position of the atom, respectively. $Q(\mathbf{q},\lambda,t)$ is the normal coordinate of mode $(\mathbf{q},\lambda)$, and $\mathbf{w}_j(\mathbf{q},\lambda)$ is a normalized eigenvector of the dynamical matrix,

$$\mathbf{D} = (m_i m_j)^{-1/2}\, (\partial^2\Phi/\partial u_i \partial u_j). \quad (15)$$

From (14) and (13) one obtains a general expression for the MSRD of a pair of atoms in harmonic approximation:

$$\sigma_j^2 = (N\mu)^{-1} \sum_{\mathbf{q},\lambda} \langle |Q(\mathbf{q},\lambda,t)|^2 \rangle\ |[\mathbf{w}_j(\mathbf{q},\lambda)\exp\,(i\mathbf{q}\cdot\mathbf{R})/(m_j/\mu)^{1/2}$$
$$-\ \mathbf{w}_0(\mathbf{q},\lambda)/(m_0/\mu)^{1/2}]\cdot\hat{\mathbf{R}}|^2, \quad (16)$$

where m_0 and m_j are the masses of the absorber and backscatterer atoms, respectively, and μ is their reduced mass. The canonical averages of the normal coordinates depend on the eigen frequencies, $\omega(\mathbf{q},\lambda)$, of the dynamical matrix $\mathbf{D}$ and on temperature,

$$\langle |Q(\mathbf{q},\lambda,t)|^2 \rangle = [\hbar/2\omega(\mathbf{q},\lambda)]\coth\,[\hbar\omega(\mathbf{q},\lambda)/2kT]. \quad (17)$$

When the square of the binomial expression inside the modulus bars in (16) is calculated, the two direct terms correspond to the uncorrelated MSD of absorber and backscatterer atoms, and the cross product corresponds to the DCF.

For a monatomic Bravais crystal the number, N, of atoms is equal to the number, N, of unit cells, all atoms have the same mass, $m = 2\mu$, and eigenvectors, and (16) reduces to

$$\sigma_j^2 = (N\mu)^{-1} \sum_{\mathbf{q},\lambda} \langle |Q(\mathbf{q},\lambda,t)|^2 \rangle$$
$$\times\ [\mathbf{w}(\mathbf{q},\lambda)\cdot\hat{\mathbf{R}}]^2[1 - \cos\,(\mathbf{q}\cdot\hat{\mathbf{R}})], \quad (18)$$

In monatomic Bravais crystals, where only acoustical modes are present, the correlation depends on the phonon wavevectors through the dot product $\mathbf{q}\cdot\mathbf{R}$. In non-Bravais crystals the phase relationships between eigenvectors can add a significant, if not predominant, contribution to correlation.
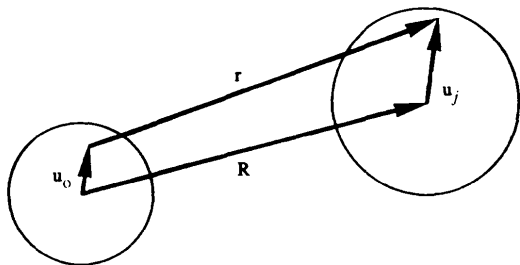

Figure 5
Schematic picture of the relation between instantaneous distance $\mathbf{r}$ and thermal displacements $\mathbf{u}_0$ and $\mathbf{u}_j$.

The EXAFS of a given coordination shell is the sum of the contributions from all atoms composing it. Using standard harmonic formula for one coordination shell, (6), one has

$$\chi(k) = \sum_j \chi_j(k) \propto \sum_j \exp\,(-2k^2\sigma_j^2)\sin\,(2kR + \varphi). \quad (19)$$

4.3. EXAFS and diffraction: correlation effects

Let us compare the Debye–Waller factor of standard EXAFS formula, $\exp\,(-2k^2\sigma^2)$, with the Debye–Waller factor of X-ray diffraction. To keep the notation simple we will consider only monatomic crystals.

The time-averaged intensity of diffracted beams can be expressed, in electronic units, as

$$I_{eu}(\mathbf{G}) = |f(\mathbf{G})|^2 \sum_{m,n} \exp\,[i\mathbf{G}\cdot(\mathbf{R}_m - \mathbf{R}_n)]$$
$$\times\ \exp\,\{-G^2\langle[\hat{\mathbf{G}}\cdot(\mathbf{u}_m - \mathbf{u}_n)]^2\rangle/2\}, \quad (20)$$

where $\mathbf{G}$ is the scattering vector, $f(\mathbf{G})$ is the atomic scattering factor, and the sum is over all atomic pairs (m,n) within the crystal. $\mathbf{R}_i$ and $\mathbf{u}_i$ $(i = m, n)$ are the equilibrium position and thermal displacement, respectively, of atom i. The last factor in (20), the *Debye–Waller factor*, has been written in a form directly comparable with that of EXAFS. In EXAFS the scattering vector has magnitude $2k$, and is directed along the bond direction $\hat{\mathbf{R}}$. The XRD exponent $\langle[\hat{\mathbf{G}}\cdot(\mathbf{u}_m - \mathbf{u}_n)]^2\rangle$, like the EXAFS exponent $\langle[\hat{\mathbf{R}}\cdot(\mathbf{u}_j - \mathbf{u}_0)]^2\rangle$, can be expanded as a sum over normal modes: an expression similar to (18) is found for the exponent of the XRD Debye–Waller factor, the distance between absorber and backscatterer neighbours $\mathbf{R}$ being replaced by the distance $\mathbf{R}_{m,n}$ between any two atoms of the crystal.

There are, however, several important differences between XRD and EXAFS. First of all, diffraction patterns carry information on average atomic displacements in all directions perpendicular to Bragg planes even for powdered samples; on the contrary, an EXAFS spectrum carries unidimensional information on the averaged atomic movements along the different bond directions of the absorber atom, and even for polarized beams and monocrystalline samples the angular sensitivity is relatively poor.

On the other hand, while the EXAFS signal of one coordination shell is the sum of the contributions of a few atoms, the XRD signal is a sum over all the (m,n) atomic pairs within the crystal. As a consequence of long-range averaging, the effect of short-range correlations is dispersed into thermal diffuse scattering. The XRD Debye–Waller factor only monitors the uncorrelated MSD.

The MSD of each atom of a crystalline powder can be obtained from X-ray diffraction measurements as

$$\langle u^2 \rangle_{\text{all dir.}} = (\text{trace }\mathbf{B})/3, \quad (21)$$

where $\mathbf{B}$ is the 3×3 *mean-square displacement matrix* (Willis & Pryor, 1975). By subtracting the sum of the MSDs of absorber and backscatterer atoms measured by XRD

from the EXAFS MSRD, one can obtain the experimental value of the correlation function DCF.

Figs. 6, 7 and 8 illustrate the effects of correlation in different systems. In general, the correlation decreases with increasing interatomic distance, and the MSRD of the outer shells progressively approaches the uncorrelated MSD. In the f.c.c. Bravais crystals of Cu and Pt only acoustical modes are present, and the correlation is accounted for by long-wavelength phonons; although absolute values of the MSRDs are quite different for the two metals, the ratios between MSRDs of the first and second shell are very similar (Fig. 6). Crystalline germanium has two atoms per primitive cell and three optical branches in addition to

the three acoustical ones. The correlation term also contains the contribution from the phase relationships between phonon eigenvectors; its effect on the first shell (Fig. 7) is proportionally stronger than in the Bravais metals.

The MSRDs plotted in Figs. 6 and 7 have been obtained by phenomenological data analyses based on the amplitude ratio method within the single-scattering and plane-wave approximations (Stern, Bunker & Heald, 1980; Dalba, Fornasini, Grazioli & Rocca, 1995). The MSRDs of the second and third shells are then biased by residual multiple scattering and spherical wave effects which are not compensated by the ratio method. However, the extent of these residual effects does not significantly modify
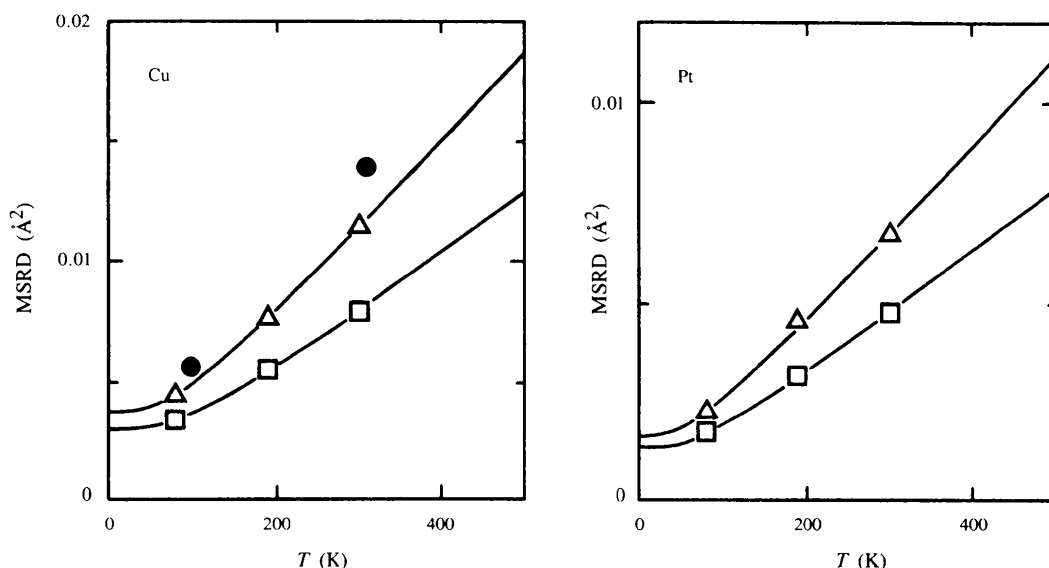

Figure 6
MSRD of the first (open squares) and second (open triangles) coordination shells of Cu and Pt as a function of temperature. Absolute values have been obtained by fitting a Debye-correlated model to the slope of experimental points measured by Stern *et al.* (1980). The full circles are MSD values from XRD measurements (Ibers, Templeton, Vainshtein, Bacon & Lonsdale, 1985).
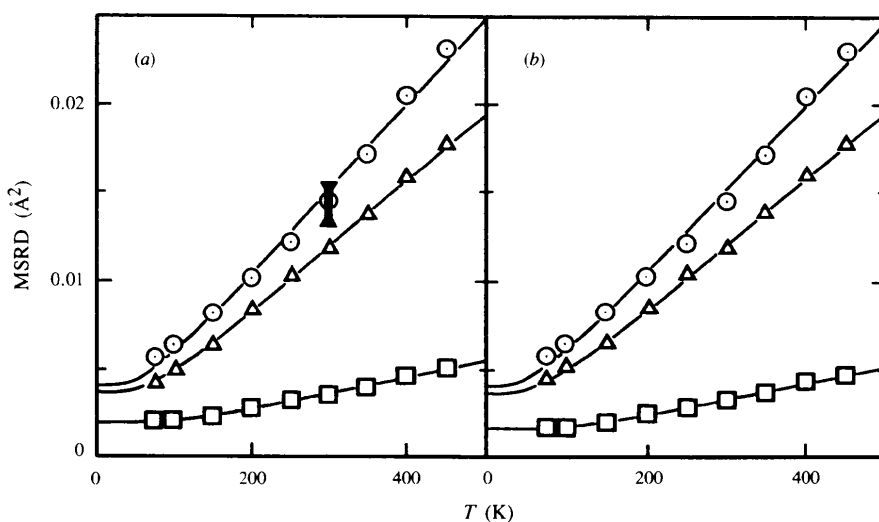

Figure 7
MRSDs of first (open squares), second (open triangles) and third (open circles) coordination shells of germanium as a function of temperature. Absolute values have been obtained by fitting correlated Einstein (*a*) or Debye (*b*) models to the slope of the experimental points (Dalba, Fornasini, Grazioli & Rocca, 1995). The vertical bar at 300 K in (*a*) represents the spread of uncorrelated MSD values calculated from available XRD data.

the basic information on correlation. As will be shown below, the MSRDs of germanium plotted in Fig. 7 are in good agreement, after subtraction of the anharmonic contributions, with recent theoretical calculations.

Correlation effects stronger than in germanium have been found in β-AgI, which has the wurtzite structure, with four atoms per primitive cell (Fig. 8). In AgI the presence of low-frequency optical modes strongly characterizes the vibrational properties; their phenomenological study helps in better understanding the possible role of optical modes in correlation (Dalba, Fornasini, Rocca & Mobilio, 1990). Fig. 9 shows the ionic displacement patterns calculated at the centre of the Brillouin zone for the 0.5 THz optical modes of AgI. Let us consider an iodine central atom. The three basal Ag atoms of the first shell move in phase with the central I atom; the apical Ag atom moves out of phase, but the atomic displacements are normal to the bond direction; as a consequence, although the MSD values of both atomic species are quite high, the contribution to the MSRD is negligible. Considering now the second shell, six of the twelve I atoms move in phase with the central atom and do not contribute to the MSRD; the other six move out of phase and their displacement vectors have a finite component along the bond direction, so we expect a non-negligible contribution to the MSRD. Otherwise stated, the low-frequency optical modes of AgI can account for large distortions of the iodine tetrahedral cage and strong displacements of the silver ion inside without affecting the I–Ag MSRD. As a consequence, EXAFS spectra of AgI are consistent not only with a liquid-like excluded-volume model, which can explain the strong Ag–I correlation only in terms of long-wavelength acoustical phonons (Hayes, Boyce & Beeby, 1978), but also with more realistic models
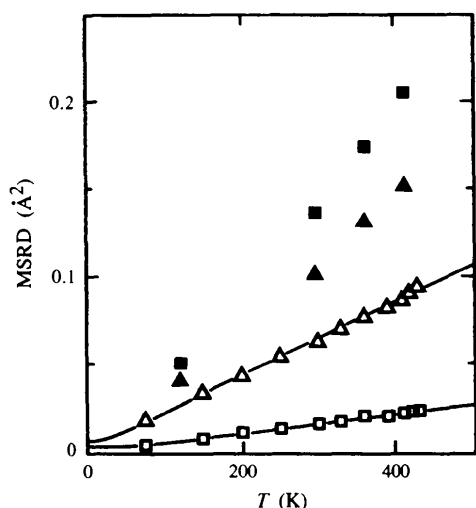
in which the ion mobility and possibly the superionic phase transition are related to vibrational dynamics (Fornasini, 1995).

4.4. Theoretical models

The calculation of the MSRD through (16) requires a full knowledge of eigenvalues and eigenvectors of the dynamical matrix. Sevillano et al. (1979) calculated the MSRD of monatomic cubic crystals of Cu, Fe and Pt from different force-constant models, finding results differing by 5–10%, and suggested that EXAFS could provide a useful test of the validity of models.

The peculiar vibrational information contained in EXAFS is the DCF, which depends, for non-Bravais crystals, on the phase relationships between eigenvectors of the dynamical matrix. It is well established that different vibrational dynamical models, though giving the same dispersion curves, can yield different eigenvectors (Cochran, 1971). In the case of AgI the temperature dependence of the experimental MSRD of first-shell I–Ag and second-shell I–I pairs could be reproduced via (16) with eigenvectors calculated at the centre of the Brillouin zone (Dalba et al., 1990). However, when the entire Brillouin zone was sampled, using eigenfrequencies and eigenvectors calculated via a valence-shell model which satisfactorily reproduced the phonon dispersion curves
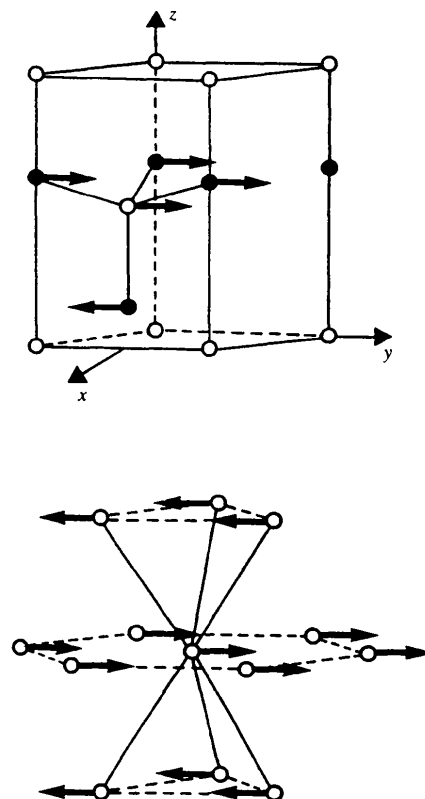

Figure 8
MSRDs of the first-shell I–Ag distance (open squares) and second-shell I–I distance (open triangles) in β-AgI as a function of temperature (Dalba et al., 1990). Absolute values have been obtained by fitting the slope of the experimental points to correlated Einstein models. Full squares and full triangles are the MSDs for the I–Ag and I–I pairs, respectively, calculated from the XRD data of Yoshiasa, Koto, Kanamaru, Emura & Horiuchi (1987).

Figure 9
Atomic displacement patterns of iodine (open circles) and silver (solid circles) corresponding to the eigenvectors of the 0.5 THz optical modes at the centre of the Brillouin zone (Dalba et al., 1990).

(Bührer, Nicklow & Brüesch, 1978), the strong correlation effects experimentally found for the MSRD could not be reproduced at all.

The phonon dynamics in harmonic approximation can be determined from first principles, through a perturbative approach to the density functional theory (Giannozzi, de Gironcoli, Pavone & Baroni, 1991). Using this method the EXAFS MSRD of the first three coordination shells of germanium have been calculated and compared (Strauch *et al.*, 1996) with the experimental data of Dalba, Fornasini, Grazioli & Rocca (1995). The agreement is good for the first shell when experimental data are fitted by an Einstein model (see below); for the outer shells a good agreement is obtained only when the anharmonic contribution to the MSRD is subtracted using the procedure which will be outlined in §5.

Recently, Loeffen & Pettifer (1996) have performed a full *ab-initio* calculation of temperature-dependent EXAFS for the zinc tetraimidazole molecular cluster, using a multiple-scattering approach tailored for the treatment of general disorder effects (Benfatto *et al.*, 1989). For the first time dynamical information determined from inelastic neutron scattering has been used in an EXAFS calculation. A coarse agreement has been obtained with experimental spectra at different temperatures. The non-negligible residual discrepancies have been attributed to the muffin tin effects of the potential.

The Debye–Waller factors of mono- and bi-atomic one-dimensional chains have been calculated by Miyanaga & Fujikawa (1994a) on the basis of *ab-initio* quantum statistical methods, considering an anharmonic Morse potential for the nearest-neighbours interaction. The low-temperature deviations from the classical behaviour of the anharmonic contribution to the MSRD and the third cumulant have been quantified. Different features have been found for the contributions of the optical and acoustical modes in the bi-atomic linear chain.

4.5. Phenomenological models

Debye or Einstein models are frequently used in EXAFS data analysis (*a*) to estimate absolute values of MSRD from the relative values determined by phenomenological analyses (*e.g.* the ratio method), and (*b*) to parametrize the Debye–Waller factor when theoretical values of amplitudes and phase shifts are used in data analysis.

4.5.1. Debye-correlated model.
The Debye-correlated model was developed for monatomic Bravais lattices by Beni & Platzman (1976) as a natural extension of the Debye models of specific heats and atomic thermal displacements.

In the Debye approximation the first Brillouin zone is substituted by a sphere of radius $q_D = (6\pi^2/V_a)^{1/3}$, where V_a is the volume per atom in the real space; three acoustical branches are considered with the same linear dispersion relation, $\omega = v_s q$. The density of vibrational states is proportional to ω^2. When the sum over the normal modes in (18) is substituted by the integral over the Debye sphere one obtains the expression for the EXAFS MSRD (Sevillano *et*

al., 1979),

$$\sigma_j^2(\omega_A, T) = (3\hbar/2\omega_A^3\mu) \int_0^{\omega_A} d\omega\, \omega \coth(\hbar\omega/2kT)$$
$$\times [1 - \sin(\omega q_D R_j^0/\omega_A)/(\omega q_D R_j^0/\omega_A)], \quad (22)$$

where $\omega_A = v_s q_D$ is the Debye cut-off frequency. The Debye temperature is $\theta_A = \hbar\omega_A/k_B$. The first term in (22) is the sum of uncorrelated MSDs of absorber and backscatterer atoms, and corresponds to the XRD Debye model. The second term is peculiar to the correlated Debye model for EXAFS, and gives the DCF. Equivalent analytical expressions for the Debye-correlated model can be found in the literature (*e.g.* Böhmer & Rabe, 1979). A Debye model specifically tailored to small metallic clusters, taking into account the low-frequency cut-off and the surface to bulk ratio, has been developed by Balerna & Mobilio (1986).

Different physical parameters, such as specific heat or atomic thermal displacements, depend in different ways on the density of vibrational states (DOS). The discrepancies between the true DOS and the DOS approximated by the Debye model can give rise to different values of Debye temperature for different parameters (Herbstein, 1961). In this paper we will label θ_D, θ_M and θ_A the Debye temperatures best fitting specific heats, XRD and X-ray absorption (EXAFS) data, respectively.

The Debye temperatures best fitting the temperature dependence of MSRDs available in the literature for the f.c.c. metals Cu and Pt are listed in Table 1. A reasonable agreement has been found between the θ_A values of the first four coordination shells, in spite of the reduced number of data points and the neglect of multiple-scattering effects in data analysis of outer shells. The θ_A values are also in agreement, within the experimental uncertainty, with the specific heat and XRD Debye temperatures. One single Debye temperature is then able to describe different physical phenomena in the case of Cu and Pt.

The use of the Debye model for non-Bravais lattices, in which optical modes are present, is questionable. Let us firstly consider a monatomic non-Bravais crystal, such as germanium, which has two atoms per primitive cell. A Debye-correlated model with an extended Brillouin zone was used to fit the temperature dependence of the MSRDs of the first three coordination shells (Dalba, Fornasini, Grazioli & Rocca, 1995). The corresponding Debye temperatures, θ_A, are listed in Table 1 for both cases of a purely harmonic fit and a fit including first-order anharmonic contributions (see §5).

In the case of germanium the Debye model is unable to describe different correlation effects for different coordination shells by one characteristic temperature. Also, the specific heat and XRD Debye temperatures are different. The EXAFS Debye temperature decreases with increasing interatomic distance, reflecting a first-shell correlation stronger than expected (see also Fig. 7b). At large distances θ_A approaches the Debye temperature, θ_M, determined from XRD, which describes the uncorrelated atomic motion. This trend is more accurately obeyed when anharmonic

Table 1

Debye temperatures (K) determined from the fit of a Debye-correlated model to the temperature dependence of MSRD available in the literature.

(a) Stern *et al.* (1980); (b) Greegor & Lytle (1979); (c) and (d) Dalba, Fornasini, Grazioli & Rocca (1995), harmonic and anharmonic analysis, respectively; (e) Dalba *et al.* (1990); (f) Dalba, Fornasini, Kuzmin *et al.* (1995). The last two lines show the available values of Debye temperatures from X-ray diffraction and from specific heat measurements.

		Cu		Pt	Ge		AgI	ReO$_3$
		(a)	(b)	(a)	(c)	(d)	(e)	(f)
EXAFS	First shell	334	325	242	431	442	156	800
	Second shell	310		228	276	312	96	
	Third shell	348		232	252	290		
	Fourth shell	312		230				344–360
XRD					290			360
Specific heat			315–343	230–240	354		157	327–460

contributions are included in the analysis: in this case θ_A never becomes lower than θ_M. No match is instead found with the specific heat Debye temperature, θ_D.

Still more questionable is the Debye approximation for a non-monatomic crystal. The differences between specific heat and XRD characteristic Debye temperatures for binary alloys have been evidenced by Horning & Staudenmann (1988). In the case of EXAFS the phase relationships between eigenvectors of the dynamical matrix can introduce further significant differences between different coordination shells. In Table 1 the examples of AgI and ReO$_3$ are reported.

4.5.2. *Einstein-correlated model.* The Einstein model for the EXAFS MSRD (Sevillano *et al.*, 1979) considers the pair of absorber and backscatterer atoms as an independent oscillator with frequency ω_E:

$$\sigma^2(\omega_E, T) = (\hbar/2\mu\omega_E) \coth(\hbar\omega_E/2kT). \quad (23)$$

(The Einstein model for specific heat and XRD considers instead the individual atoms as independent oscillators.)

The Einstein-correlated model is particularly suited to monitor intramolecular vibrational modes in molecular or quasimolecular crystals. Yang, Paesler & Sayers (1987) studied the MSRD of As–As and As–S pairs in arsenic and some arsenic chalcogen compounds. They found a satisfactory agreement between Einstein frequencies and Raman symmetrical stretching frequencies, concluding that the MSRD was dominated by optical stretching modes.

Also for some f.c.c. metals, where no optical modes are present, Knapp *et al.* (1985) found that the EXAFS MSRD could be fitted by an Einstein model, whose frequency was to a good approximation equal to the square root of the second moment of the phonon density of states.

In general, the Einstein frequency does not correspond to defined peaks of the density of states. It can be considered a measure of the effective bond-stretching force constant, $f = \mu\omega_E^2$. Its value can be utilized to estimate and compare the strength of different bonds.

4.5.3. *Comparison of Einstein and Debye models.* The superiority of the Debye model over the Einstein model for interpreting the temperature dependence of specific heats is well established. In the case of the EXAFS MSRD,

however, the correlation of vibrational motion plays a fundamental role, and a specifically tailored approach has to be used. The Debye-correlated model is particularly suited when only acoustical modes are present. The Einstein-correlated model better describes the effects of optical modes. In general, one considers the Einstein model superior for the first shell of non-Bravais crystals, the Debye model for the outer shells (Stern, 1988). In the case of AgI, however, it has been found that the low-frequency optical modes have much more of an effect on the second-shell than the first-shell MRSD (Fig. 9).

An exhaustive test of the relative merits of the two models is still lacking. A theoretical investigation on the Einstein and Debye models for one-dimensional chains including anharmonicity effects has been recently performed by Miyanaga & Fujikawa (1994b): for monatomic chains the Debye model gave good results even for the third and fourth cumulants, while for diatomic chains a mixed Einstein–Debye model was appropriate for the harmonic MSRD but unable to account for anharmonic cumulants.

The usual accuracy of EXAFS experiments and data analyses (which seldom take into account anharmonicity effects) hardly enables one to appreciate the differences between the two models. By imposing the high-temperature classical harmonic behaviour, $\sigma^2 \propto T$, to the MSRD it can be shown that the Einstein and Debye temperatures are connected through the relationship

$$\theta_E = \theta_A/(3S)^{1/2},$$

$$S = \sum_{n=1}^{\infty} (q_D R)^{2n}(-1)^{n+1} \Big/ [(2n+1)(2n+1)!]. \quad (24)$$

A non-negligible difference can be found at low temperatures, particularly for small $q_D R$ values, the Einstein models giving higher MSRD values than the Debye model (Dalba, Fornasini, Kuzmin *et al.*, 1995).

When, as it is common practice, an Einstein or Debye model is fitted to the temperature dependence of experimental points, different absolute values can be found for the two models. For germanium (Fig. 7) the difference is significant only for the first coordination shell. Fig. 10 gives an enlarged picture of the Einstein- and Debye-correlated

models best fitting the slopes of first-shell experimental data from the ratio method (Dalba, Fornasini, Grazioli & Rocca, 1995). The Einstein model is in good agreement, both in slope and absolute values, with the *ab-initio* calculations of Strauch *et al.* (1996). Also in Fig. 10 the MSRD values obtained by Filipponi & Di Cicco (1995) using calculated backscattering amplitudes and phase shifts are reported for comparison.

5. Anharmonicity effects

The vibrational properties of crystalline solids which are relevant to EXAFS (eigenvalues and eigenvectors of the dynamical matrix) are generally calculated, *ab-initio* or from force-constant models, in harmonic approximation. Accordingly, in the previous sections a treatment of the MSRD in harmonic approximation was made. It is well established, however, that anharmonicity effects should be taken into account in EXAFS analysis not only when dealing with highly disordered systems, such as CuBr (Tranquada & Ingalls, 1983) or AgI (Dalba *et al.*, 1993), but also for relatively ordered systems, such as Ge (Dalba, Fornasini, Grazioli & Rocca, 1995), GaAs (Dalba, Diop, Fornasini & Rocca, 1994) or ZnSe (Diop & Grisenti, 1995).

In this section we show a simple approximate method for determining and subtracting the first-order anharmonic contribution to the MSRD. The method is based on the cumulant analysis of experimental EXAFS spectra and relies on classical approximation for third and fourth cumulants. We assume that the low-temperature quantum deviations of the third and fourth cumulants from the classical behaviour (Miyanaga & Fujikawa, 1994*a*) are

Figure 10
MSRD of the first shell of germanium. Absolute values obtained by fitting an Einstein-correlated (circles) or a Debye-correlated (squares) model to the temperature dependence of experimental points obtained from the ratio method (Dalba, Fornasini, Grazioli & Rocca, 1995). The two models differ by about 15% at $T = 0$ K. The triangles are the values obtained by Filipponi & Di Cicco (1995) using calculated backscattering amplitudes and phase shifts.

negligible with respect to typical experimental uncertainty.

The distributions of interatomic distances sampled by EXAFS can be connected to an *effective pair potential*, V_e (Dalba, Fornasini, Gotter & Rocca, 1995; Yokoyama, Kobayashi, Ohta & Ugawa, 1996; Yokoyama, Yonamoto, Ohta & Ugawa, 1996). The deviation of the distributions from Gaussian shapes is reflected in the anharmonicity of the potential V_e, which can be expanded as

$$V_e(u) = au^2/2 + bu^3 + cu^4 + \ldots , \qquad (25)$$

where u is the variation of interatomic distance with respect to the potential minimum. The effective pair potential, V_e, depends on the statistically averaged behaviour of all the atoms in the crystal; its anharmonicity reflects not only the physically relevant anharmonicity of the crystal potential but also the asymmetry artificially generated when the tridimensional distributions of two thermal ellipsoids are reduced to the unidimensional distribution of distances sampled by EXAFS (Fig. 1).

In the classical approximation the first four cumulants C_i of the effective distribution of distances $P(r, \lambda)$ can be related to the force constants $a, b, c, \ldots$ of the effective potential V_e by (Tranquada & Ingalls, 1983; Stern, Livins & Zhang, 1991)

$$\delta C_1 = -(3b/a^2)k_B T + \ldots \qquad (26)$$

$$C_2 = (k_B T/a) + (k_B T/a)^2[(6b/a)^2 - (12c/a)] + \ldots \qquad (27)$$

$$C_3 = -(k_B T/a)^2(6b/a) + \ldots \qquad (28)$$

$$C_4 = (k_B T/a)^3[(108b^2/a)^2 - (24c/a)] + \ldots . \qquad (29)$$

In the expression of the MSRD C_2, the first term on the right, representing the harmonic contribution, can be substituted by an Einstein model, (23), which takes into account quantum effects, and whose frequency is connected to the force constant a by $a = \mu\omega_E^2$; the second term, representing the lowest-order anharmonic contribution, can be expressed as a function of the cumulants C_3 and C_4. The final result is

$$C_2(T) = \sigma^2(\omega_E, T) - \tfrac{1}{2}(k_B T/\mu\omega_E^2)^2 C_3^2(T)$$
$$+ \tfrac{1}{2}(k_B T/\mu\omega_E^2)C_4(T). \qquad (30)$$

If the third and fourth cumulants are known with good accuracy from experimental data, (30) contains only one free parameter, ω_E, and can be fitted to the slope of the experimental points $\Delta C_2(T)$, allowing the separation of the harmonic MSRD from the first-order anharmonic contribution.

The analysis based on (30) was applied to the MSRDs of the first three coordination shells of germanium. A fit to the experimental values better than the one given by the purely harmonic Debye or Einstein models was obtained, especially for the second and third shells, where anharmonicity effects are stronger (Fig. 11). The Einstein frequencies obtained from (30) have been connected to
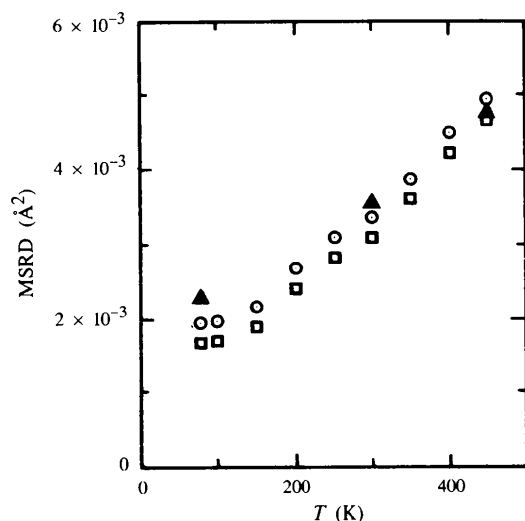
Debye temperatures through the asymptotic relation of (24); the Debye temperatures determined in this way (Table 1, column d) are more consistent with the XRD Debye temperature than those determined from a purely harmonic analysis (Table 1, column c).

The harmonic contributions to the MSRDs of germanium determined from experiment (dashed lines in Fig. 11) were shown by Dalba, Fornasini, Grazioli & Rocca (1995) to be in good agreement in slope and absolute values with the calculations of Nielsen & Weber (1980), based on a bond charge model, and of Filipponi (1988), based on the high-temperature expansion of the projected density of vibrational states. More recently, a good agreement has been found also with *ab-initio* calculations of vibrational properties (Strauch *et al.*, 1996).

6. Conclusions

The EXAFS Debye–Waller factor of crystals, like the XRD Debye–Waller factor, can be expressed as a sum of contributions of all normal vibrational modes within the Brillouin zone. The peculiar information contained in EXAFS concerns the correlation of vibrational motion. The reproduction of the temperature dependence of the
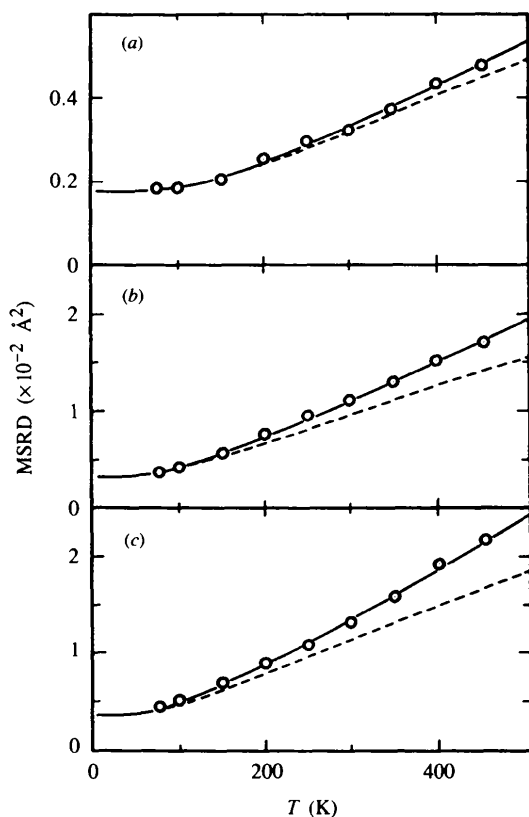

Figure 11
MSRD of the first (a), second (b) and third (c) coordination shells of germanium. The temperature dependence of the experimental ΔC_2 values (circles) has been fitted by equation (29), taking into account anharmonicity effects (continuous line). The dashed line is the harmonic term.

MSRD measured by EXAFS is an important test for the phase relationship between eigenvectors of the dynamical matrix, calculated from force-constant models or from first principles.

For Bravais crystals the correlation is referable only to long-wavelength acoustical modes; for non-Bravais crystals the role of optical modes can be determinant. In some cases, such as AgI, useful information on the properties of optical modes has been obtained directly from a phenomenological comparison of the correlation for different coordination shells.

The approximate Debye- or Einstein-correlated models are often used to describe the temperature dependence of the MSRD. The use of the Debye-correlated model for non-Bravais crystals (even if monatomic like germanium) is not trivial; different Debye temperatures can be found for different coordination shells, whose values approximate the XRD Debye temperature for large interatomic distances, while no match can be found with the specific heat Debye temperature. The frequency determined by the much simpler Einstein-correlated mode, although generally not corresponding to definite peaks of the density of vibrational states, gives direct information on the effective bond-stretching force constant. The study of the relative merits of Einstein and Debye models by comparison with more refined dynamical calculations, although highly desirable, up to now has been limited only to a few simple systems.

The study of the effects of thermal disorder on EXAFS can greatly benefit from the cumulant method. The analysis based on the cumulant expansion allows one to monitor the growth with temperature of the anharmonicity effects and to decide the adequacy of the standard formula. It is also possible to perform an evaluation of the anharmonic contribution to the MSRD and subtract it from the experimental values to obtain data directly comparable with the harmonic theoretical calculations. More refined information can be obtained in principle from the study of cumulants, in particular concerning thermal expansion. It is, however, necessarily a preliminary work for understanding the origin of the anharmonicity of the EXAFS effective pair potential and its relation with the anharmonicity of the crystal potential.

The calibration of EXAFS on vibrational properties of relatively well characterized crystalline solids should promote a more systematic use of EXAFS for the study of local vibrational properties of non-crystalline solids. One advantage of EXAFS in this field of investigations is the sensitivity to short-range correlations, which, unlike XRD, produces comparable spectra for non-crystalline systems as well as their crystalline equivalents. Another advantage is the relative quickness of temperature-dependent EXAFS measurements.

References

Balerna, A. & Mobilio, S. (1986). *Phys. Rev. B*, **34**, 2293-2298.

Benfatto, M., Natoli, C. R. & Filipponi, A. (1989). *Phys. Rev. B*, **40**, 9626-9635.

Beni, G. & Platzman, P. M. (1976). *Phys. Rev. B*, **14**, 1514-1518.

Böhmer, W. & Rabe, P. (1979). *J. Phys. C*, **12**, 2465-2474.

Brouder, C. (1988). *J. Phys. C*, **21**, 5075-5086.

Brüesch, P. (1982). *Phonons: Theory and Experiments*, Vol. 1. Berlin: Springer-Verlag.

Bührer, W., Nicklow, R. M. & Brüesch, P. (1978). *Phys. Rev. B*, **17**, 3362-3370.

Bunker, G. (1983). *Nucl. Instrum. Methods*, **207**, 437-444.

Busing, W. R. & Levy, H. A. (1964). *Acta Cryst.* **17**, 142-146.

Cochran, W. (1971). *Acta Cryst.* A**27**, 556-559.

Crozier, E. D., Rehr, J. J. & Ingalls, R. (1988). In *X-ray Absorption*, edited by D. C. Koningsberger & R. Prins. New York: Wiley.

Dalba, G., Diop, D., Fornasini, P., Grisenti, R., Pasqualini, D., Rocca, F. & Traverse, A. (1996). *J. Phys. (Paris)*. In the press.

Dalba, G., Diop, D., Fornasini, P. & Rocca, F. (1994). *J. Phys. Condens. Matter*, **6**, 3599-3608.

Dalba, G., Fornasini, P., Gotter, R. & Rocca, F. (1995). *Phys. Rev. B*, **52**, 149-157.

Dalba, G., Fornasini, P., Grazioli, M. & Rocca, F. (1995). *Phys. Rev. B*, **52**, 11034-11043.

Dalba, G., Fornasini, P., Kuzmin, A., Purans, J. & Rocca, F. (1995). *J. Phys. Condens. Matter*, **7**, 1199-1213.

Dalba, G., Fornasini, P. & Rocca, F. (1993). *Phys. Rev. B*, **47**, 8502-8514.

Dalba, G., Fornasini, F., Rocca, F. & Mobilio, S. (1990). *Phys. Rev. B*, **41**, 9668-9675.

Diop, D. & Grisenti, R. (1995). *Physica B*, **208/209**, 164-166.

Eisenberger, P. & Brown, G. S. (1979). *Solid State Commun.* **29**, 481-484.

Filipponi, A. (1988). *Phys. Rev. B*, **37**, 7027-7037.

Filipponi, A. & Di Cicco, A. (1995). *Phys. Rev. B*, **51**, 12322-12336.

Fornasini, P. (1995). *Nucl. Instrum. Methods Phys. Res. B*, **97**, 70-74.

Fujikawa, T. & Miyanaga, T. (1993). *J. Phys. Soc. Jpn*, **62**, 4108-4122.

Fujikawa, T., Yimagawa, M. & Miyanaga, T. (1995). *J. Phys. Soc. Jpn*, **64**, 2047-2068.

Giannozzi, P., de Gironcoli, S., Pavone, P. & Baroni, S. (1991). *Phys. Rev. B*, **43**, 7231-7242.

Gnedenko, B. V. (1976). *The Theory of Probability*. Moscow: MIR.

Greegor, R. B. & Lytle, F. W. (1979). *Phys. Rev. B*, **20**, 4902-4907.

Hayes, T. M., Boyce, J. B. & Beeby, J. L. (1978). *J. Phys. C*, **11**, 2931-2937.

Herbstein, F. H. (1961). *Adv. Phys.* **10**, 313-355.

Horning, R. D. & Staudenmann, J. L. (1988). *Acta Cryst.* A**44**, 136-142.

Ibers, J. A., Templeton, D. H., Vainshtein, B. K., Bacon, G. E. & Lonsdale, K. (1985). In *International Tables for X-ray Crystallography*, Vol. III. Dordrecht: Reidel.

Ishii, T. (1992). *J. Phys. Condens. Matter*, **4**, 8029-8034.

Knapp, G. S., Pan, H. K. & Tranquada, J. M. (1985). *Phys. Rev. B*, **32**, 2006-2009.

Lee, P. A., Citrin, P. H., Eisenberger, P. & Kincaid, B. M. (1981). *Rev. Mod. Phys.* **53**, 769-806.

Loeffen, P. W. & Pettifer, R. F. (1996). *Phys. Rev. Lett.* **76**, 636-639.

Miyanaga, T. & Fujikawa, T. (1994a). *J. Phys. Soc. Jpn*, **63**, 1036-1052.

Miyanaga, T. & Fujikawa, T. (1994b). *J. Phys. Soc. Jpn*, **63**, 3683-3690.

Nielsen, O. H. & Weber, W. (1980). *J. Phys. C*, **13**, 2449-2460.

Ono, I., Yokoyama, H., Sato, H., Kaneyuki, K. & Ohta, T. (1992). *Jpn. J. Appl. Phys.* **32**, 83-85.

Rennert, P. (1992). *J. Phys. Condens. Matter*, **4**, 4315-4322.

Sandstrom, D. R., Marques, E. C., Biebesheimer, V. A., Lytle, F. W. & Greegor, R. B. (1985). *Phys. Rev. B*, **32**, 3541-3548.

Sevillano, E., Meuth, H. & Rehr, J. J. (1979). *Phys. Rev. B*, **20**, 4908-4911.

Shmidt, V. V. (1961). *Bull. Acad. Sci. USSR Phys. Ser.* **25**, 988-993.

Shmidt, V. V. (1963). *Bull. Acad. Sci. USSR Phys. Ser.* **27**, 392-397.

Stern, E. A. (1988). In *X-ray Absorption*, edited by D. C. Koningsberger & R. Prins. New York: Wiley.

Stern, E. A., Bunker, B. A. & Heald, S. M. (1980). *Phys. Rev. B*, **21**, 5521-5539.

Stern, E. A., Livins, P. & Zhang, Z. (1991). *Phys. Rev. B*, **43**, 8850-8860.

Stern, E. A., Ma, Y., Hanske-Petitpierre, O. & Bouldin, C. E. (1992). *Phys. Rev. B*, **46**, 687-694.

Strauch, D., Pavone, P., Nerb, N., Karch, K., Windl, W., Dalba, G. & Fornasini, P. (1996). *Physica B*, **219/220**, 436-438.

Tranquada, J. M. & Ingalls, R. (1983). *Phys. Rev. B*, **28**, 3520-3528.

Tröger, L., Yokoyama, T., Arvanitis, D., Lederer, T., Tischer, M. & Baberschke, K. (1994). *Phys. Rev. B*, **49**, 888-903.

Willis, B. T. M. & Pryor, A. W. (1975). *Thermal Vibrations in Crystallography*. Cambridge University Press.

Yang, C. Y., Paesler, M. A. & Sayers, D. E. (1987). *Phys. Rev. B*, **36**, 980-988.

Yokoyama, T., Kobayashi, K., Ohta, T. & Ugawa, A. (1996). *Phys. Rev. B*, **53**, 6111-6122.

Yokoyama, T., Yonamoto, Y., Ohta, T. & Ugawa, A. (1996). *Phys. Rev. B*, **54**, 6921-6928.

Yoshiasa, A., Koto, K., Kanamaru, F., Emura, S. & Horiuchi, H. (1987). *Acta Cryst.* B**43**, 434-440.